J. Fluid Mech. (2011), *vol.* 686, *pp.* 484–506.
doi:10.1017/jfm.2011.341

Plane Poiseuille flow of miscible layers with different viscosities: instabilities in the Stokes flow regime

L. Talon[1,2] **and E. Meiburg**[2]†

[1] Laboratoire Fluides Automatique et Systèmes Thermiques, Université Pierre et Marie Curie, CNRS (UMR 7608) Bâtiment 502, Campus Universitaire, 91405 Orsay CEDEX, France

[2] Department of Mechanical Engineering, University of California at Santa Barbara, Santa Barbara, CA 93106, USA

(Received 15 September 2010; revised 5 May 2011; accepted 6 August 2011; first published online 26 September 2011)

We investigate the linear stability of miscible, viscosity-layered Poiseuille flow. In the Stokes flow regime, diffusion is observed to have a destabilizing effect very similar to that of inertia in finite-Reynolds-number flows. For two-layer flows, four types of instability can dominate, depending on the interface location. Two interfacial modes exhibit large growth rates, while two additional bulk modes grow more slowly. Three-layer Stokes flows give rise to diffusive modes for each interface. These two diffusive interface modes can be in resonance, thereby enhancing the growth rate. Furthermore, modes without inertia and diffusion are also observed, consistent with a previous long-wave analysis for sharp interfaces. In contrast to that earlier investigation, the present analysis demonstrates that instability can also occur when the more viscous layer is in the centre, at larger wavenumbers.

Key words: core–annular flow, instability, low-Reynolds-number flows

1. Introduction

The stability of flows with viscosity stratification has been widely investigated, motivated by such industrial processes as pipeline lubrication, polymer deposition and extrusion. Since the pioneering work of Yih (1967), it has been known that Couette–Poiseuille flows with step-like viscosity stratification are unstable for arbitrarily small positive Reynolds numbers. This is in contrast to single-fluid Couette–Poiseuille flows, which require a critical value of the Reynolds number to trigger an instability (see Lin 1955). However, both types of flow share the property that inertia is required for instabilities to develop. The present investigation will demonstrate that for miscible flows with viscosity stratification, instabilities can develop even in the Stokes regime, as a result of diffusive effects.

Our investigation will focus on two-dimensional Poiseuille flows (see figure 1) which are driven by a mean pressure gradient and bounded by no-slip walls. We will occasionally refer to related stability results for other, similar configurations, such as those of Couette type, where the flow is driven by a wall moving at a constant velocity, or Couette–Poiseuille type, which involve both a pressure drop and a moving wall. Axisymmetric core–annular flows have also been widely investigated, due to

† Email address for correspondence: meiburg@engineering.ucsb.edu

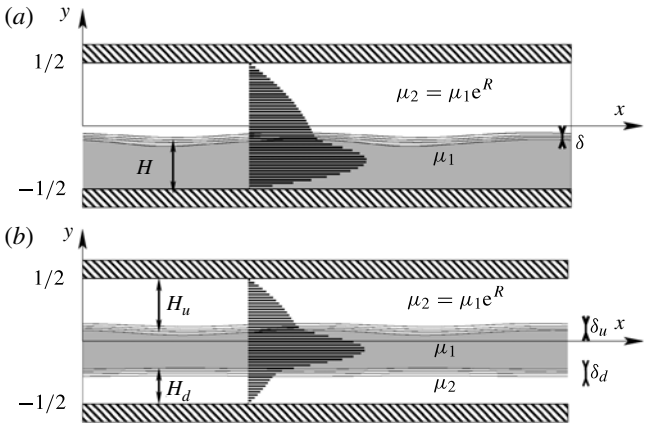

FIGURE 1. Sketch of two-layer (*a*) and three-layer (*b*) plane Poiseuille flow. The fluids have different viscosities and are miscible with each other. The base state velocity fields are indicated by the horizontal bars.

their relevance to industrial applications. The so-called half-Poiseuille configuration, in which the pressure-driven flow is bounded by one no-slip and one slip wall, is related. It corresponds to the symmetric three-layered case with $H_u = H_d$ in figure 1(*b*).

The stability of single-fluid, plane Poiseuille flow has been the subject of numerous studies in the literature (see Drazin & Reid 1981 and Schmid & Henningson 2001 for reviews). As mentioned earlier, here the Reynolds number must exceed a critical value for the flow to become unstable. For such flows, the instability is controlled by the critical layer in the flow, where the fluid velocity $U(y)$ is equal to the phase velocity c_ϕ of the disturbance. In this region the viscosity term is most important, since the term in the Orr–Sommerfeld equation with the $(U(y) - c_\phi)$ prefactor vanishes, and the remaining inertial term also vanishes in the long-wave limit. This instability mode is usually referred to as the Tollmien–Schlichting or 'bulk' mode. We also mention the work by Wall & Wilson (1996), who investigated the influence on the stability of the viscosity variation due to a temperature gradient in the channel. The author reported that, while the Péclet number has little influence on the instability, the base state viscosity distribution does influence the Tollmien–Schlichting mode. Consistent with this observation, this type of instability mode is modified for non-Newtonian fluids (Nouar & Frigaard 2009). The stability of Couette–Poiseuille flows with viscosity stratification was first studied by Yih (1967). In the long-wave approximation, he showed that two viscous fluids separated by a sharp interface result in unstable flow for any positive Reynolds number, however small. Follow-up investigations since then have addressed many aspects of this inertial interfacial instability. Among them are the work of Hooper & Boyd (1983) for unbounded two-dimensional shear flows, and the investigation by Hinch (1984) into the physical instability mechanism for short waves. The latter author argues that inertia induces a phase shift of the vorticity on both sides of the interface, which destabilizes the system. Also relevant is the numerical investigation by Yiantsios & Higgins (1988), who provide stability results for two-layered Poiseuille flows with buoyancy. A physical instability mechanism has also been proposed by Charru & Hinch (2000), based on their investigation of bounded and unbounded Couette flow.

The first axisymmetric Poiseuille flow investigation by Hickox (1971) was later extended by Renardy (1987), who accounted for the influence of surface tension and a density difference (see Joseph & Renardy 1992*a*,*b*). Three-layer Couette flows were analysed by Li (1969) and Kliakhandler & Sivashinsky (1995). We will find below that this case is particularly interesting, as it leads to instability even for vanishing Reynolds number, i.e. in the absence of inertia.

Miscibility of the fluids primarily affects the stability properties of the flow by causing the interface to be of finite width, so the viscosity distribution is smooth. Furthermore, the interface thickness evolves in time. Except for the investigation by Craik (1969), to be discussed below, stability analyses of miscible flows with viscosity stratification are more recent. Originally, miscible flows were thought to have stability properties similar to those of their immiscible counterparts. Molecular diffusion was assumed to stabilize the flow somewhat, by reducing the initial viscosity contrast and damping any instabilities that might arise: e.g. Scoffoni, Lajeunesse & Homsy (2001). However, these assumptions were shown to be invalid by Ern, Charru & Luchini (2003), who investigated the influence of the Péclet number on interfacial instabilities in Couette flows. Specifically, they showed diffusion to have a non-monotonic influence on the growth rate, so flows at intermediate Péclet numbers can be more unstable than those without diffusion (infinite Péclet numbers). For symmetric three-layer Poiseuille flows, Ranganathan & Govindarajan (2001) and Govindarajan (2004) discussed the role of the thin, intermediate viscosity layer created by miscibility. If this layer coincides with the location of the Tollmien–Schlichting critical layer, the flow may become more stable or unstable, depending on the viscosity ratio. In particular, it can become unstable at Reynolds numbers much lower than for the corresponding immiscible configuration. A similar result was obtained by Malik & Hooper (2005), who showed that in the case of a two-layered system, when the critical layer is located within the width of the interface (treated as a third layer), the system gives rise to an interfacial instability. We emphasize that in the above cases, inertia is still required to drive the instability. Moreover, diffusion has little influence on the instability beyond causing the base state to have a finite width interfacial region. As a case in point, Malik & Hooper (2005) analyse the flow as an immiscible three-layer system.

Craik (1969) highlights several interesting aspects of miscible stability problems. Specifically, he points out that the linearized advection–diffusion equation for the concentration field (see below) has a structure similar to that of the Orr–Sommerfeld equation. In particular, it has a corresponding term with a prefactor $(U(y) - c_\phi)$. The author argues that this should lead to the existence of a critical diffusive layer, in which diffusion cannot be neglected. Hence one should obtain 'diffusive' modes, analogous to the 'viscous' modes found by Lin (1955), by replacing Re with Pe. Using this analogy, Craik predicts that for two-layered Couette flow one should observe a Yih-like instability if the diffusive critical layer coincides with a region where the second derivative of the base flow velocity is negative. One of the goals of the present investigation will be to elucidate whether or not the critical layer is of particular significance for miscible flows with viscosity stratification.

Recently, Selvam *et al.* (2007) numerically investigated inertial instabilities of miscible core annular flow. Interestingly, they observe that the flow can be unstable in the Stokes flow limit. This finding partially motivates the current investigation into Stokes flow instabilities of miscible two-layered or three-layered Poiseuille flows. Section 2 formulates the governing equations, derives the relevant linear stability problem and briefly comments on the numerical procedure for its solution. Section 3

describes the linear stability findings for two-layered systems. Four modes are shown to exist, and their dependence on the governing parameters will be discussed. Section 4 provides corresponding results for three-layered systems. Specifically, it discusses the existence of Stokes flow instabilities in light of the reversibility of the Stokes equations. Finally, § 5 summarizes the main findings of the investigation.

2. Governing equations and numerical approach

We assume that the velocity $\boldsymbol{u} = (u, v)$ and the concentration field c are governed by the dimensionless system of equations

$$\nabla \cdot \boldsymbol{u} = 0, \tag{2.1}$$

$$Re\left(\frac{\partial \boldsymbol{u}}{\partial t} + \boldsymbol{u} \cdot \nabla \boldsymbol{u}\right) = -\nabla p + \nabla \cdot \boldsymbol{\tau}, \tag{2.2}$$

$$\frac{\partial c}{\partial t} + \boldsymbol{u} \cdot \nabla c = \frac{1}{Pe}\Delta c, \tag{2.3}$$

where p denotes the pressure and $\boldsymbol{\tau}$ represents the Newtonian stress tensor. Here we have introduced characteristic length, velocity, time and pressure scales of the form

$$L^* = e, \quad U^* = U, \quad T^* = \frac{e}{U}, \quad P^* = \frac{\mu_1 U}{e}, \tag{2.4}$$

where e indicates the channel width and U the mean flow velocity, respectively. We furthermore assume an exponential dependence of the viscosity on the concentration

$$\mu(c) = \mu_1 \mathrm{e}^{Rc} \quad \text{with } R = \ln \mu_2/\mu_1, \tag{2.5}$$

where μ_1 and μ_2 denote the dynamic viscosities of the two fluids. The Reynolds and Péclet numbers are defined as

$$Re = \frac{Ue}{\mu_1}, \tag{2.6}$$

$$Pe = \frac{Ue}{D}, \tag{2.7}$$

and represent, as usual, the ratio of advective to diffusive transport of momentum and concentration, respectively. We impose no-slip velocity boundary conditions at the walls, along with the condition of vanishing concentration flux across the walls.

In the usual way, we perform the stability analysis by linearizing equations (2.1)–(2.3) around a steady, uniform base state that depends on y only:

$$p(x, y, t) = \bar{p}(y) + p'(x, y, t), \tag{2.8}$$

$$u(x, y, t) = \bar{u}(y) + u'(x, y, t), \tag{2.9}$$

$$v(x, y, t) = v'(x, y, t), \tag{2.10}$$

$$c(x, y, t) = \bar{c}(y) + c'(x, y, t). \tag{2.11}$$

For two-layer flows, we will focus on concentration base states of error function shape

$$\bar{c}(y) = \frac{1}{2} + \frac{1}{2}\mathrm{erf}\left(\frac{y - y_0}{\delta}\right), \tag{2.12}$$

where y_0 represents the interface position and δ denotes the width of the diffused base state. Correspondingly, in the three-layered systems we have

$$\bar{c}(y) = 1 - \frac{1}{2}\mathrm{erf}\left(\frac{y - y_d}{\delta_d}\right) + \frac{1}{2}\mathrm{erf}\left(\frac{y - y_u}{\delta_u}\right), \tag{2.13}$$

where y_u and y_d indicate the upper and lower interface locations with the respective thicknesses δ_u and δ_d. Following the analysis by Yang & Yortsos (1997), the unidirectional velocity base state $\bar{u}(y)$ can be evaluated as

$$\bar{u}(y) = \frac{G(y)}{\displaystyle\int_{-0.5}^{0.5} G(y')\,\mathrm{d}y'}, \tag{2.14}$$

where

$$G(y) = \int_{-0.5}^{0.5} \lambda(y')\,\mathrm{d}y' \int_{-0.5}^{y} \lambda(y')y'\,\mathrm{d}y' - \int_{-0.5}^{0.5} \lambda(y')y'\,\mathrm{d}y' \int_{-0.5}^{y} \lambda(y')\,\mathrm{d}y', \tag{2.15}$$

and $\lambda(y) = \mu_1^{-1}\mathrm{e}^{-R\bar{c}(y)}$. We remark that the parallel flow assumption clearly represents a certain idealization, as in a real flow one would expect to have a diffuse interface whose thickness varies in the streamwise distance. However, a parallel flow appears to be a well-suited first step for analysing miscible flows in the Stokes limit. It avoids the complication of analysing non-parallel flow effects, which might obfuscate the fundamental physical mechanisms underlying the instability.

We assume a normal mode decomposition of the perturbations of the form

$$\begin{pmatrix} p' \\ u' \\ v' \\ c' \end{pmatrix} = \begin{pmatrix} \hat{P}(y) \\ \hat{U}(y) \\ \hat{V}(y) \\ \hat{C}(y) \end{pmatrix} \mathrm{e}^{\mathrm{i}(\alpha x - \omega t)}. \tag{2.16}$$

We thus obtain a generalized eigenvalue problem

$$\boldsymbol{A}\boldsymbol{\phi} = -\omega \boldsymbol{B}\boldsymbol{\phi}, \tag{2.17}$$

where the operators $\boldsymbol{A}$, $\boldsymbol{B}$ and the vector $\boldsymbol{\phi}$ are defined by

$$\boldsymbol{A} = \begin{pmatrix} 0 & \mathrm{i}\alpha \boldsymbol{I} & \partial_y & 0 \\ -\mathrm{i}\alpha \boldsymbol{I} & \boldsymbol{M_1} & \boldsymbol{M_6} & \boldsymbol{M_2} \\ -\partial_y & 0 & \boldsymbol{M_3} & \boldsymbol{M_4} \\ 0 & 0 & \dfrac{\partial \bar{c}}{\partial y}\boldsymbol{I} & \boldsymbol{M_5} \end{pmatrix}, \quad \boldsymbol{B} = \begin{pmatrix} 0 & 0 & 0 & 0 & 0 \\ 0 & 0 & \mathrm{i}\,Re & 0 & 0 \\ 0 & 0 & 0 & \mathrm{i}\,Re & 0 \\ 0 & 0 & 0 & 0 & \mathrm{i} \end{pmatrix} \tag{2.18a}$$

and

$$\boldsymbol{\phi} = \begin{pmatrix} \hat{P} \\ \hat{U} \\ \hat{V} \\ \hat{C} \end{pmatrix}, \tag{2.18b}$$

with

$$\boldsymbol{M_1} = [-\alpha^2 \mathrm{e}^{R\bar{c}} - \mathrm{i}\,Re\,\bar{u}\alpha]\boldsymbol{I} + R\,\mathrm{e}^{R\bar{c}}\frac{\partial \bar{c}}{\partial y}\partial_y + \mathrm{e}^{R\bar{c}}\partial_{yy}, \tag{2.19}$$

$$\boldsymbol{M_2} = \mathrm{e}^{R\bar{c}} R \left(R \frac{\partial \bar{u}}{\partial y} \frac{\partial \bar{c}}{\partial y} + \frac{\partial^2 \bar{u}}{\partial y^2} \right) \boldsymbol{I} + \mathrm{e}^{R\bar{c}} R \frac{\partial \bar{u}}{\partial y} \boldsymbol{\partial_y} \tag{2.20}$$

$$\boldsymbol{M_3} = -\alpha^2 \mathrm{e}^{R\bar{c}} \boldsymbol{I} - \mathrm{i}\alpha Re\, \bar{u} \boldsymbol{I} + 2\mathrm{e}^{R\bar{c}} R \frac{\partial \bar{c}}{\partial y} \boldsymbol{\partial_y} + \mathrm{e}^{R\bar{c}} \boldsymbol{\partial_{yy}}, \tag{2.21}$$

$$\boldsymbol{M_4} = \mathrm{i}\alpha \mathrm{e}^{R\bar{c}} \frac{\partial \bar{u}}{\partial y} R \boldsymbol{I}, \tag{2.22}$$

$$\boldsymbol{M_5} = \left(-\mathrm{i}\alpha \bar{u} - \alpha^2 \frac{1}{Pe} \right) \boldsymbol{I} + \frac{1}{Pe} \boldsymbol{\partial_{yy}}, \tag{2.23}$$

$$\boldsymbol{M_6} = \left(\mathrm{i}\alpha R\, \mathrm{e}^{R\bar{c}} \frac{\partial \bar{c}}{\partial y} - Re \frac{\partial \bar{u}}{\partial y} \right) \boldsymbol{I}, \tag{2.24}$$

where $\boldsymbol{I}$ represents the identity matrix; $\boldsymbol{\partial_y}$ and $\boldsymbol{\partial_{yy}}$ denote the first and second derivatives in the y-direction, which we discretize by means of the sixth-order compact finite difference derivative operator (see Lele 1992) on a regular grid. For the sake of efficiency, in the two-layered case, we also sometimes use a collocation Chebyshev method to discretize on a non-uniform mesh refined around the interface (analogous to the one used by Govindarajan 2004). The grid size was adapted (more points for thin interfaces) to reduce the error to below 0.1 %. The complex eigenvalue ω is subsequently calculated via standard MATLAB routines.

We thus obtain the growth rate $\sigma(\alpha) = \mathrm{Im}(\omega)$ and phase velocity $c_\phi(\alpha) = \omega/\alpha$ as a function of the wavenumber α, for all perturbation modes. In the following, we will denote by σ_M the maximum growth rate of all modes, and by α_M the wavenumber at which it occurs.

We remark that, if one had used a streamfunction formalism, the first three lines of (2.17) would have led to the classical Orr–Sommerfeld equation (e.g. Govindarajan 2004). In contrast, in the inertialess regime ($Re = 0$) it is primarily the last equation, which is derived from the linearized concentration equation, that determines the growth rate (though coupled with the flow equation)

$$\frac{\partial \bar{c}}{\partial y} \hat{V} - \mathrm{i}\alpha (\bar{u}(y) - c_\phi) \hat{C} - \alpha^2 \frac{1}{Pe} \hat{C} + \frac{1}{Pe} \boldsymbol{\partial_{yy}} \hat{C} = 0. \tag{2.25}$$

Following Craik (1969), we emphasize the fact that, in the long-wave limit (i.e. neglecting the α^2 term), this eigenproblem is very similar to the Orr–Sommerfeld problem. The solutions are controlled by the critical layer, the position y_c at which $\bar{u}(y_c) = c_\phi$. Solutions of this eigenproblem should thus be very similar to the viscous solution studied by Lin (1955) if we replace Re by Pe.

To summarize, the governing parameters of our problem are the viscosity ratio R, the Péclet number Pe, and the Reynolds number Re, in addition to the interface locations and thicknesses, respectively.

3. Two-layer system

In this section, we will discuss linear stability results for plane Poiseuille flow of two fluid layers miscible with each other; see figure 1(*a*).

3.1. *Eigenspectra at large Reynolds numbers*

Building on the discussion in South & Hooper (1999), we compare in figure 2 the eigenspectra (noting $c_r = \mathrm{Re}(c_\phi)$ and $c_i = \mathrm{Im}(c_\phi)$) for the cases $R = 0$ (no viscosity contrast) and $R = 2.5$ at $Re = 10^3$. In the absence of a viscosity contrast, we obtain

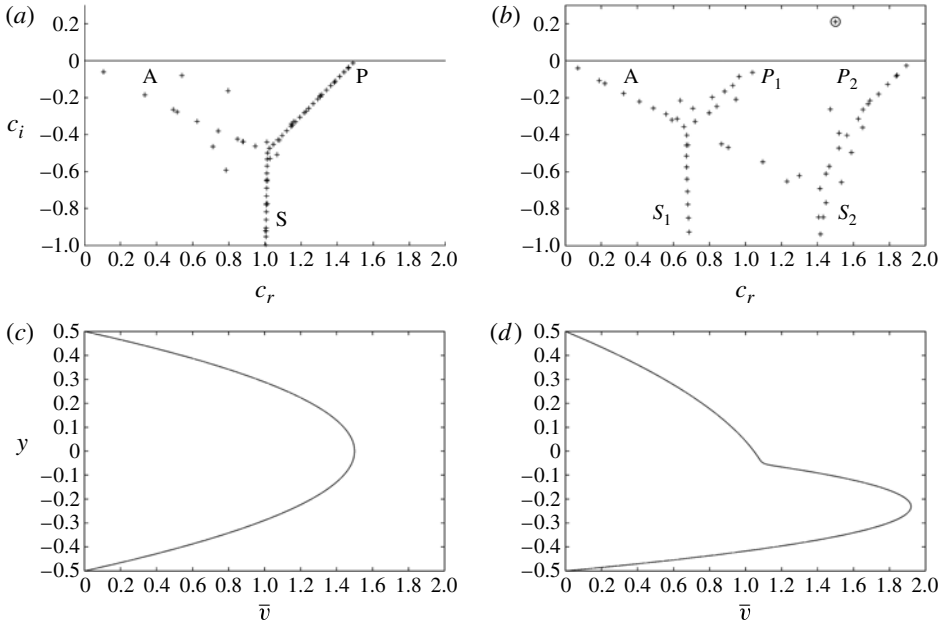

FIGURE 2. Eigenspectra (*a, b*) and velocity profiles (*c, d*) for $Pe = 10^4$, $Re = 10^3$, $\delta = 0.01$, $\alpha = 2$ and $H_d = 0.45$. (*a, c*) The two layers have the same viscosity ($R = 0$). (*b, d*) The two layers have different viscosities ($R = 2.5$).

the classical Y-shaped eigenspectrum for plane Poiseuille flow, with the A, P and S branches (Mack 1976). A closer comparison with the eigenspectrum obtained by South & Hooper (1999) for corresponding immiscible two-layer flow, however, reveals that for the present, miscible case a significantly larger number of modes exists on each of those branches. Hence, we conclude that these new modes originate from the convection–diffusion equation. This is easily confirmed by varying the Péclet number, which results in a shift of those additional modes.

When we introduce a viscosity contrast between the two layers, several features emerge that correspond to the observations of South & Hooper (1999) for immiscible flows (figure 2). Most importantly, an unstable mode (encircled) appears in the upper plane $c_i > 0$, attributed to an interfacial instability mode, and the *S*-branch splits into two new branches (denoted S_1 and S_2). The additional splitting of the *P*-branch was not observed by South & Hooper (1999), which may indicate that it is associated with the convection–diffusion equation. We note that the two new branches P_1 and P_2 appear to intersect the real axis at values close to the interface velocity ($c_r \sim 1.1$) and the maximum flow velocity ($c_r \sim 1.9$), respectively.

Figure 3 indicates that the majority of the modes remain unchanged as the Reynolds number is reduced to zero, confirming that they are associated with the concentration equation. Most importantly, as *Re* approaches zero the unstable mode remains in the upper plane, which indicates that the instability is not primarily due to inertial effects. In the following, we will investigate this instability mode at $Re = 0$, with a focus on the contribution of the advection–diffusion equation.

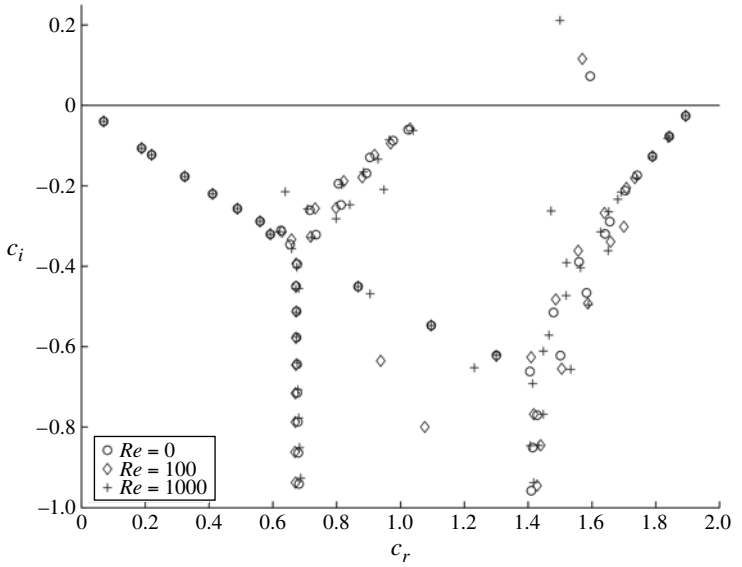

FIGURE 3. Eigenspectra for $Pe = 10^4$, $R = 2.5$, $\alpha = 2$ and $H = 0.45$ for different Re numbers. As Re is reduced to zero, the unstable mode remains in the upper plane.

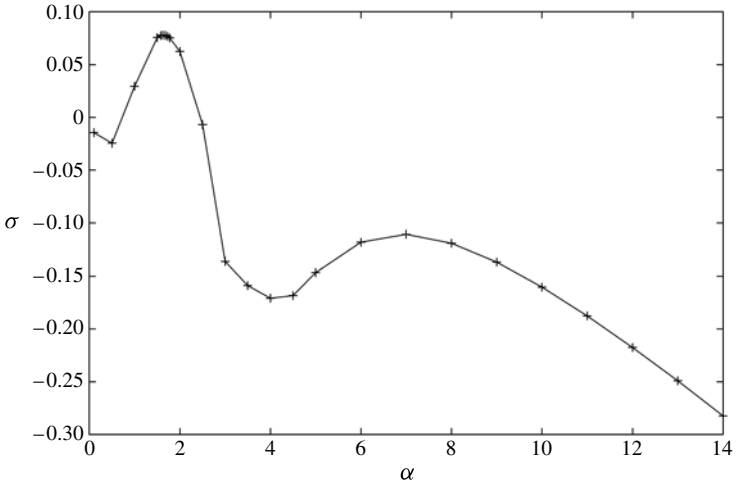

FIGURE 4. Representative dispersion relation $\sigma(\alpha)$ of the most unstable mode. The parameters are $Re = 0$, $R = 2.5$, $Pe = 2 \times 10^3$, $H = 0.45$ and $\delta = 0.01$.

3.2. *Influence of interface location and viscosity contrast*

Figure 4 shows a typical dispersion relation $\sigma(\alpha)$ for $Re = 0$. From curves such as this, we can obtain the most unstable wavenumber α_M and its growth rate σ_M, as functions of the fluid layer thickness H and the interface thickness δ.

Figure 5 illustrates how σ_M varies with the fluid layer thickness H, for different viscosity ratios R. The growth rate is seen to depend strongly on the interface position, and it generally reaches its highest values for interfaces located close to the cell centre, but shifted towards the side of the less viscous fluid. σ_M generally increases with the

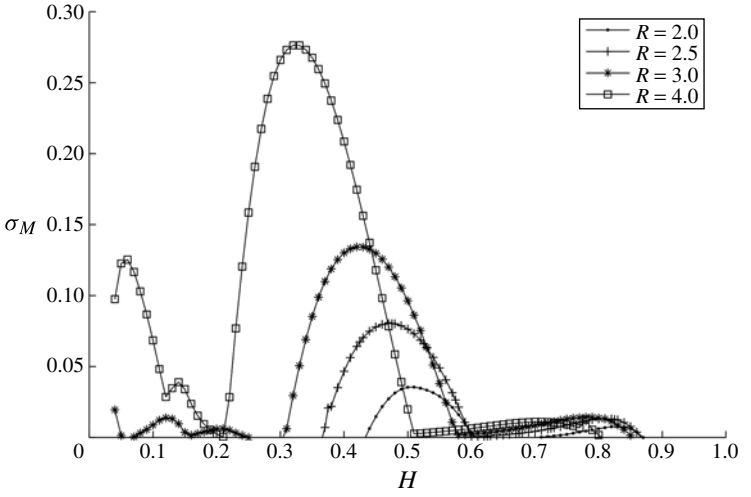

FIGURE 5. Maximum growth rate σ_M as function of the interface location, for different viscosity ratios R. The other parameters are $Re = 0$, $Pe = 2 \times 10^3$ and $\delta = 0.01$.

viscosity contrast. Above $R > 3$, a strong maximum in the growth rate arises for small values of H, i.e. for relatively thin layers of the less viscous fluid. This observation is in contrast to the well-known 'thin viscous effect', which associates a thin layer of less viscous fluid with a stabilization of the interface (see Renardy 1987).

The instability modes can be characterized more precisely by comparing their phase velocity to the velocity at the interface location, as well as to the maximum velocity of the entire profile. Figure 6 allows us to distinguish four regions of instability for $R = 4$.

I_1: The most unstable range of interface locations is given by $H \in [0.2; 0.5]$. In this range, the phase velocity of the instability is significantly larger than the fluid velocity at the interface. Eigenfunction streamline plots (figure 7) reveal two counter-rotating vortices at the same x-location, one centred at the interface and the other located entirely within the less viscous fluid.

I_2: The second unstable range occurs for $H \in [0; 0.13]$. It has a phase velocity much smaller than the interface velocity, and it is characterized by only one vortex centred at the interface location.

B_1: A third unstable range $H \in [0.13; 0.2]$ is characterized by a phase velocity larger than the maximum base flow velocity. While this may be surprising at first glance, we recall that Joseph (1968) (see also Drazin & Reid 1981) reports that the phase velocity is bounded by a value higher than the maximum fluid velocity. The instability mode involves a single vortex, which is centred inside the more viscous fluid but extends across the whole domain.

B_2: A final unstable mode occurs in the range $H \in [0.5; 0.8]$. This mode is characterized by a small phase velocity (see figure 6) and a single vortex centred inside the less viscous fluid.

In summary, for large viscosity contrasts we observe four distinct regimes of instability at $Re = 0$, depending on the thickness of the less viscous fluid layer. Two of these modes are associated with interfacial instabilities, while the other two indicate bulk flow instabilities. We note that for intermediate viscosity ratios, e.g. $R = 2.5$, the

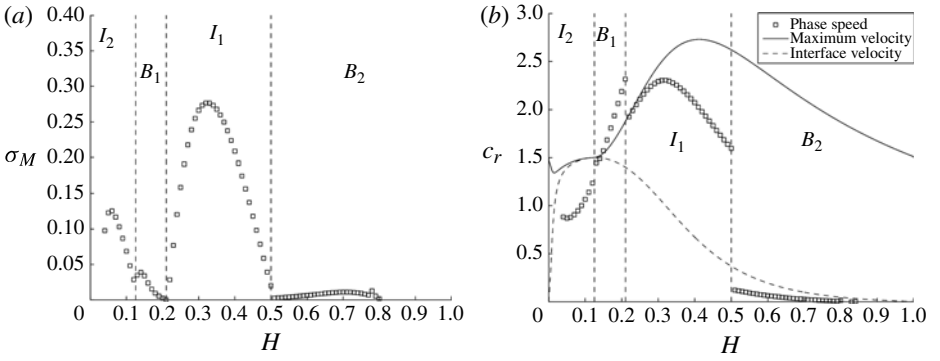

FIGURE 6. Growth rate (*a*) and phase velocity (*b*) for the most dangerous mode as functions of interface location and viscosity ratio, for $R = 4$, $Re = 0$, $Pe = 2 \times 10^3$, and $\delta = 0.01$. The dashed and solid curves correspond to the velocity at the interface and the maximum flow velocity, respectively.

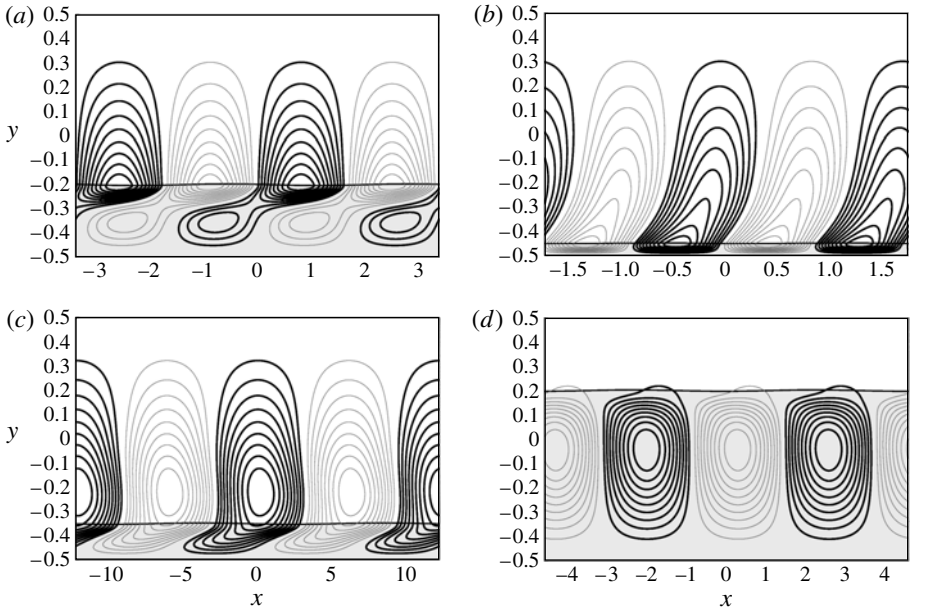

FIGURE 7. Examples of the most unstable mode eigenvectors for $R = 4$, $Pe = 2 \times 10^3$, $Re = 0$. The contour lines represent the perturbed streamline (thick line for anticlockwise and thin for clockwise). (*a*) I_1-mode, $H = 0.3$ and $\alpha = 1.8653$. (*b*) I_2-mode, $H = 0.05$ and $\alpha = 4.0444$. (*c*) B_1-mode, $H = 0.15$ and $\alpha = 0.5137$. (*d*) B_2-mode, $H = 0.7$ and $\alpha = 1.3445$.

I_2- and B_1-modes are stable. Interestingly, for most conditions the phase velocity of the instability is quite distinct from the velocity at the interface location. This suggests that the mechanism described by Govindarajan (2004), which involves an interaction between the critical layer and the mixed layer, may not be applicable here.

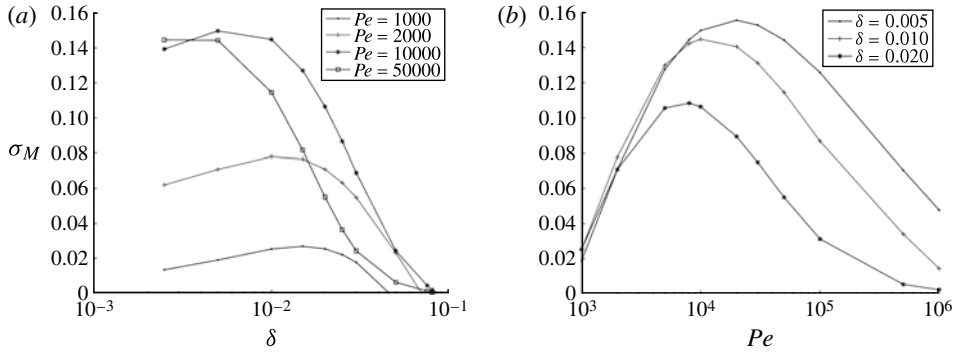

FIGURE 8. Maximum growth rate for different values of the interface thickness (a) and the Pe number (b). The other parameters are $Re = 0$, $R = 2.5$, $H = 0.45$.

3.3. *Influence of the Péclet number and interface thickness*

We now focus on the effects of miscibility, as characterized by the parameters Pe and δ. Figure 8 shows the maximum growth rate σ_M as a function of the interface thickness and the Péclet number for an interface position corresponding to the main mode of instability I_1. The graphs indicate that both δ and Pe have a non-monotonic influence on the instability, in the following sense. For a given value of Pe, an intermediate interface thickness exists for which the growth rate is maximized, while in the two limits $\delta \to 0$ or ∞ the growth rate approaches zero. Similarly, for a given value of the interface thickness, the growth rate attains a maximum for an intermediate value of the Péclet number, with the two limits $Pe \to 0$ or ∞ showing $\sigma_M \to 0$. The results for these limits are consistent with our expectations. $Pe \to 0$ means that the interface is diffusing much faster than it is being advected, so we would expect diffusion to damp any perturbations. In the other limit, $Pe \to \infty$, diffusion is absent, so one should recover the limiting case of the classical interfacial instability described by Yih (1967) and Malik & Hooper (2005), for which $\sigma \propto Re$, with $Re = 0$ in our case.

Figure 9 displays the influence of the interface thickness and the Péclet number on the maximum growth rate σ_M for different interface locations. We note that primarily the interfacial modes I_1 and I_2 are affected by those two parameters, while the influence on the B_2-mode is relatively minor. For moderately large Péclet numbers, the I_2-mode that was stable at $Pe = 2 \times 10^3$ becomes the dominant mode. However, as the Péclet number increases further, the growth rates of all modes begin to decline. We remark that we expect the growth rates to tend to zero for $Pe \to \infty$, as the effects of miscibility are reduced. Due to numerical limitations, however, this limit could not be studied in detail within the present investigation.

3.4. *Influence of the Reynolds number*

Figure 10 displays the maximum growth rate σ_M as a function of the interface location for several distinct Re values. The Reynolds number is seen to affect only the I_1-mode. Figure 10(b) indicates that the increase in σ_M with Re is approximately linear. This mode is thus continuously affected by the Reynolds number and by the parameters Pe and δ, reflecting the miscibility of the fluids. This finding is in agreement with the observation made in § 3.1, where we showed that the diffusive and inertial instabilities in fact correspond to the same interfacial mode.

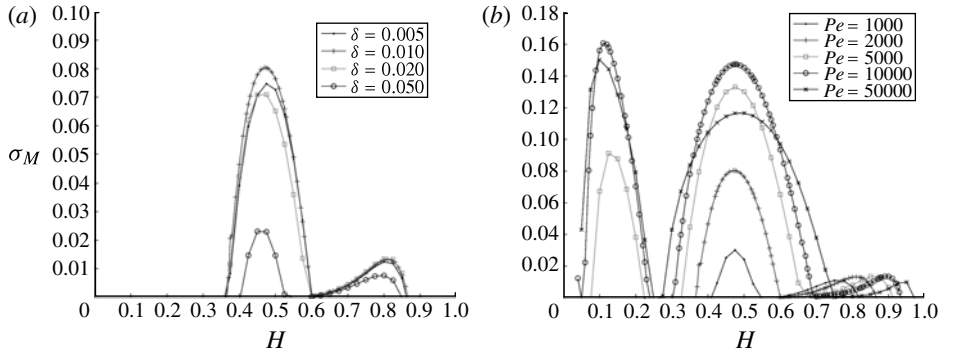

FIGURE 9. Maximum growth rate σ_M as a function of the interface location, for different interface thicknesses (*a*), with $Pe = 2 \times 10^3$, and Péclet numbers (*b*), with $\delta = 0.01$. The other parameter values are $Re = 0$, $R = 2.5$.

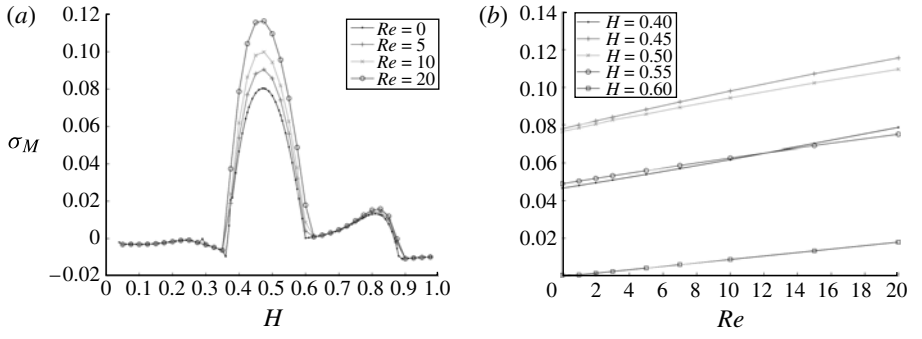

FIGURE 10. Maximum growth rate as a function of the interface location, for several different Reynolds numbers. The other parameter values are $R = 2.5$, $Pe = 2 \times 10^3$ and $\delta = 0.01$.

3.5. *Instability mechanism*

In order to identify the mechanism behind the growth of the instability, we need to understand how a wavy perturbation of the interface results in the formation of perturbation vorticity. Furthermore, as was already argued by Hinch (1984), the maxima and minima of the vertical velocity field induced by this perturbation vorticity need to exhibit a phase shift with regard to the maxima and minima of the interface perturbation. Only if such a phase shift exists will the crests and valleys of the interface move upwards and downwards, respectively, so that the initial perturbation will grow. Hinch showed that for finite-Reynolds-number flows this phase shift is generated as a result of fluid inertia. In the current Stokes flow situation, fluid inertia is absent, so that a different mechanism must exist for the generation of the phase shift between the interface and vorticity perturbations.

The base flow has a sharp change in slope at the interface, due to the different viscosities. Let us assume a situation where we have less viscous fluid at the bottom, and more viscous fluid above: see figure 11. Hinch (1984), in his figure 1, explains that a wavy perturbation to the interface results in the formation of perturbation vorticity of the sign shown in figure 11(*b*), as a result of the condition that the velocity has to be continuous at the perturbed interface location. This perturbation

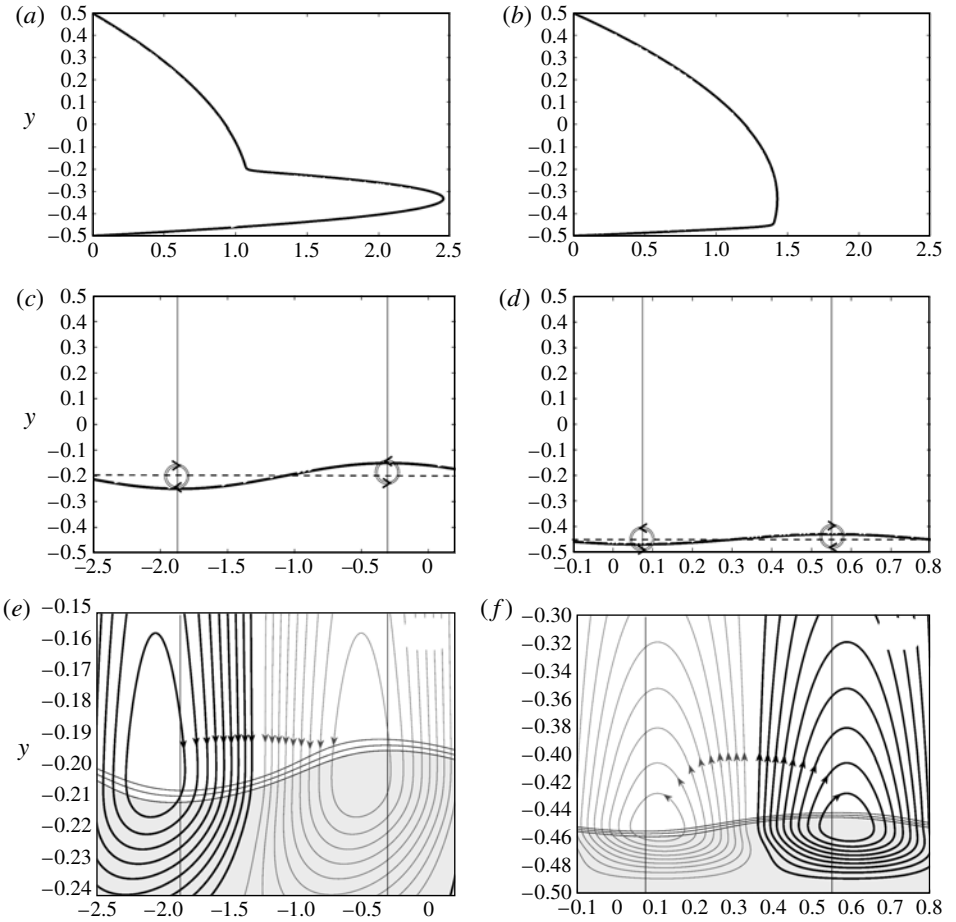

FIGURE 11. Velocity profile for $H = 0.3$ (a) and $H = 0.05$ (b). (c, d) Sketch of the perturbed vorticity generated near the crests and valleys of a sinusoidal interface perturbation, deduced from the velocity profile. (e,f) Perturbed streamline contours. The vertical lines mark the valleys and crests of the interface perturbation. One can clearly see that the vertical velocity field induced by the perturbation vorticity is shifted upstream (downstream) with regard to the interface perturbation for the I_1-mode (I_2-mode).

vorticity is clearly visible in the corresponding streamfunction eigenfunction shown in figure 11(c). The continuity of the shear stress at the interface causes this perturbation vorticity to be larger in the less viscous layer. For finite-Reynolds-number flows, Hinch then proceeds to argue that this vorticity perturbation is convectively transported, so it develops a phase shift with regard to the interface perturbation, thus enabling the interface perturbation to grow.

In the absence of fluid inertia, vorticity cannot be convectively transported, so the Hinch mechanism cannot lead to instability in the Stokes flow limit. However, it is important to keep in mind that for miscible fluid flow, as a result of diffusion across the interface, some of the less viscous fluid moves above the interface, and some of the more viscous fluid moves below the interface, thereby modifying the viscosity profile. As a result of interface curvature, the details of this diffusion process will

be slightly different where the interface is perturbed upward rather than downward. Consequently, the local concentration perturbation will be different at those two locations. The convective terms in the concentration equation will now shift this perturbation concentration relative to the interface perturbation. Since the perturbation vorticity is a direct consequence of the perturbation concentration (i.e. the perturbation viscosity), this convective transport of the perturbation concentration will result in the phase shift between vorticity and interface perturbation that is required for the interface perturbation to grow: see figure 11(*c*). We recognize that the perturbation velocity points upward at the location of the interface crest and downward at the valley, so that the interface perturbation is amplified. To summarize, for miscible fluid flows in the Stokes limit the convective terms in the concentration equation can have an effect that corresponds to that of the inertial terms for finite-Reynolds-number immiscible flows, as far as the generation of a phase shift is concerned.

The above argument also explains why the instability is non-monotonic in the Péclet number. Convection is required to create the phase shift between the concentration and the interface perturbations, but one also needs diffusion so that fluid can cross the interface in the first place. Hence the instability disappears for both vanishing and infinite Péclet numbers.

Let us now consider the corresponding figure 11(*d–f*) for the I_2-mode. We note that the curvature of the base velocity profile at the interface is opposite to the I_1-mode of figure 11(*a*). Hence the perturbation vorticity is now clockwise at the crest and anticlockwise in the valley, i.e. opposite to the I_1-mode, and the phase shift between interface and vorticity perturbation is of the opposite sign as well.

3.6. *Discussion*

The above results indicate the existence of four distinct instability modes in the Stokes flow regime. The two most rapidly growing modes are interfacial in nature. The results demonstrate that both Re and Pe continuously modify the growth of the same mode, which seems to indicate that molecular diffusion acts similarly to fluid momentum diffusion (viscosity) for small Re numbers. We remark that, since the growth rate of the inertial instability is proportional to the Reynolds number while the growth rate of the diffusive mode has an upper bound, the contribution of molecular diffusion to the interfacial instability is dominant only at low Reynolds numbers (for $Re \lesssim 10$) and comparatively large Péclet numbers, i.e. at large Schmidt numbers. This raises the question as to how important these effects are in real-world applications. Recall that for a given fluid the Schmidt number $Sc = Pe/Re$ is constant, e.g. $Sc \sim 10^3$ for water. For $Pe = 2 \times 10^3$ we obtain $Re \sim 2$, which lies in a range where the molecular diffusion contribution is significant (see figure 10). Thus, in experiments at Reynolds numbers of the order of unity (such as in d'Olce *et al.* 2008, for instance) one should expect a significant contribution of the molecular diffusion to the destabilization.

We remark that the instability modes described above probably also occur for miscible fluid layers in the Couette configuration. In this context, the investigation by Ern *et al.* (2003) is relevant. For miscible shear instabilities at $Re = 0.25$, these authors show that the growth rate displays a non-monotonic behaviour with Pe, exhibiting a maximum around $Pe \sim 10^3$. Moreover, in the limit $Pe \to \infty$, the growth rate tends to the limit of the discontinuous two-layer flow. In light of the present results, their observations are probably due to the superposition of a constant inertial contribution and the diffusion effects analysed here.

4. Three-layer system

We now focus on plane Poiseuille flows with two miscible interfaces, as depicted in figure 1. For this configuration, inertial instabilities have been extensively investigated in two dimensions, e.g. Yih (1967), Joseph & Renardy (1992*a*,*b*) and Govindarajan (2004) and others, whereas Stokes flows received comparatively little attention in the past.

4.1. *Stokes flow instability in the absence of diffusion*

The earlier investigations by Li (1969), Kliakhandler & Sivashinsky (1995) and Talon *et al.* (2004) show that, for the case of long waves in a non-symmetrical, three-layered system, the two sharp interfaces may interact to produce an instability. Remarkably, this instability exists in the absence of inertia and diffusion. Shariati *et al.* (2004) and Talon *et al.* (2004) discuss this instability in terms of the change of type of the conservation equations from hyperbolic to elliptic. Neglecting diffusion, the conservation of mass in the upper and lower layers can be written as

$$\frac{\partial H_u}{\partial t} + \frac{\partial F_u}{\partial x} = 0 \quad \text{and} \quad \frac{\partial H_d}{\partial t} + \frac{\partial F_d}{\partial x} = 0, \tag{4.1}$$

where H_u and H_d denote the upper and lower layer thicknesses, and F_u and F_d represent the corresponding volume fluxes. Using quasi-parallel flow approximation, one can show that F_d and F_u depend only on H_u and H_d, as the height of the middle layer can be expressed in terms of H_u and H_d. Consequently, (4.1) can be rewritten as

$$\frac{\partial}{\partial t}\begin{pmatrix} H_u \\ H_d \end{pmatrix} + \begin{pmatrix} M_{11} & M_{12} \\ M_{21} & M_{22} \end{pmatrix} \cdot \frac{\partial}{\partial x}\begin{pmatrix} H_u \\ H_d \end{pmatrix} = \begin{pmatrix} 0 \\ 0 \end{pmatrix}, \tag{4.2}$$

where the matrix $\boldsymbol{M}$ is real and depends on H_u and H_d only.

It is straightforward to show that the eigenvalues of the matrix $\boldsymbol{M}$ represent the complex velocity of a long-wave perturbation. The fact that the matrix is real is of importance with respect to the stability of the flow, since only two possibilities exist: either the system is hyperbolic, in which case both eigenvalues are real, so the flow is marginally stable for long waves, or the system is elliptic, which means the two eigenvalues are complex (and necessarily conjugate), so the flow is unstable. Note that the flow can never be strictly stable, since if the eigenvalue of one mode has a negative imaginary part, that of the other mode has a positive imaginary part. In light of the following discussion, we remark that these instabilities always exhibit a phase shift between the two interfaces.

It is of interest to discuss the above type of instability in light of the reversibility of the flow equations. Hinch (1984) points out that for Stokes flow in the absence of diffusion, if the horizontal flow direction is reversed, the vertical direction is reversed as well, so one should return to the initial state. Since the stability properties of the flow should not depend on the horizontal flow direction, the author argues that Stokes flow should be stable, and that inertia is required for instability to occur. However, the above equation shows that even a reversible equation can give rise to instability, in the absence of inertia and diffusion, as a result of $\boldsymbol{M}$ being real, i.e. the existence of two complementary modes. For a given horizontal flow direction, one of the two modes will be stable, while the other one is unstable. If the flow direction is reversed, the previously stable (unstable) mode will now be unstable (stable). Hence, one can return to the initial state, even though unstable modes exist, so the reversibility of the equation is not incompatible with the existence of an instability, if all of the modes

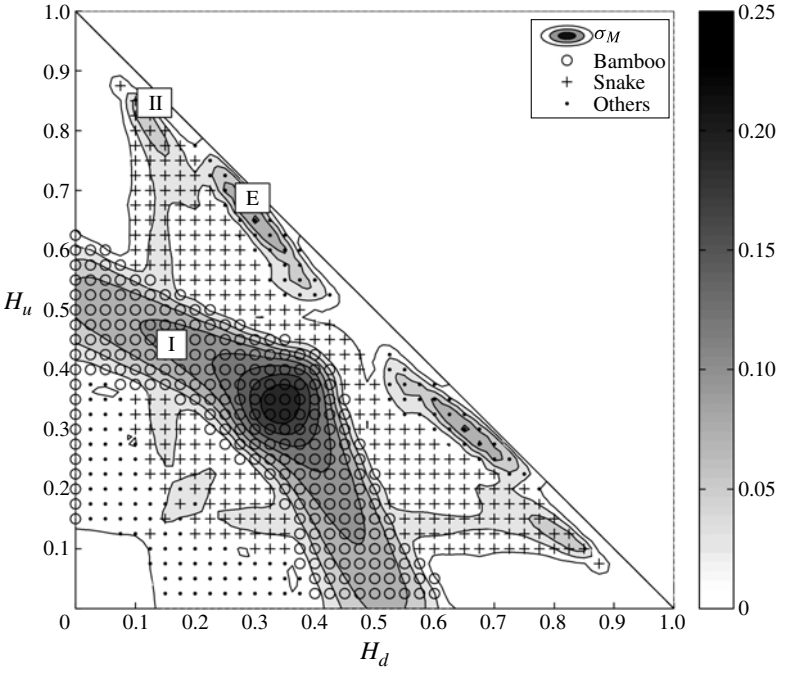

FIGURE 12. Growth rate of the most unstable mode as a function of the upper and lower fluid layer thicknesses. The parameters are $R = 2.5$, $Re = 0$, $Pe = 2{,}000$ and $\delta_u = \delta_d = 0.01$. Symbols denote unstable states.

are taken into account. However, since we need at least two modes for this instability to arise, we conclude that at least two interfaces are required. This is one reason why immiscible, two-layered Stokes flows of Poiseuille or Couette type are always marginally stable.

4.2. *Results*

Figure 12 shows the stability diagram as a function of the upper and lower fluid layer heights, H_u and H_d. The other parameters are $R = 2.5$, $Re = 0$, $\delta_u = \delta_d = 0.01$ and $Pe = 2{,}000$. The grey-level contours represent the growth rate. We note that, due to the symmetry of the problem, the diagram is symmetrical with respect to the line $H_u = H_d$. Symbols indicate the type of the dominant instability mode, according to one of three categories. When the upper and lower interface oscillations are in phase, the mode is said to be of 'snake' type. When they have opposite phases, we term it to be of 'bamboo' type. Finally, modes that do not show either of those characteristics are simply referred to as 'other'.

While most combinations of H_u and H_d result in weakly unstable flow, figure 12 allows us to identify five islands of strong instability. The dominant island of instability, denoted by 'I', is of bamboo type and represents a diffusive interface mode. The streamfunction eigenmode (see figure 13*a*), indicates a shape that is very similar to the I_1 mode of the previous section. A main region of closed streamlines is centred at the interface closest to the channel centreline, while a counter-rotating region is located at the same x-location inside the less viscous fluid. We remark that these closed streamlines of course exist only for the perturbation streamfunction and not the complete streamline (addition of the base and perturbed flow).

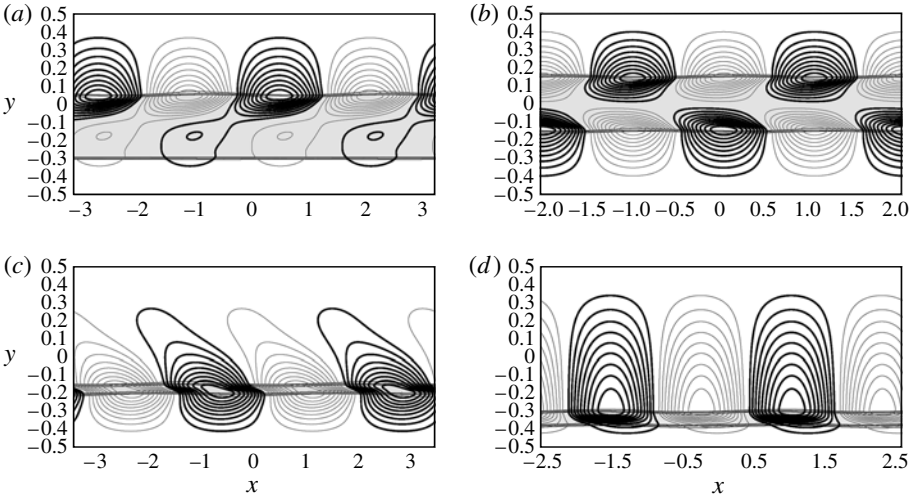

FIGURE 13. Streamfunction eigenmodes for different parameter combinations. Parameter values: $Re = 0$, $R = 2.5$, $Pe = 2{,}000$, $\delta_u = \delta_d = 0.01$. (*a*) I-mode, $(H_d; H_u) = (0.2; 0.45)$, $\alpha_M = 1.9799$. (*b*) I-mode, $(H_d; H_u) = (0.35; 0.35)$, $\alpha_M = 3.0266$. (*c*) E-mode, $(H_d; H_u) = (0.3; 0.65)$, $\alpha_M = 1.8191$. (*d*) II-mode, $(H_d; H_u) = (0.125; 0.8)$, $\alpha_M = 2.3757$.

Figure 14 shows the corresponding stability diagram for $\delta_u = 0.04$ and $\delta_d = 0.01$. The contours are no longer symmetrical, and growth rates in the upper half of the 'I'-island have significantly decreased. This dependence on the interface thickness confirms that the mode is diffusive. We can furthermore conclude that the upper (lower) section of the 'I'-island reflects the instability of the upper (lower) interface, which indicates that the interface located further away from the wall is the more unstable one.

We note that for symmetrical cases $H_d = H_u$ the growth rate can be amplified through a 'resonance' mechanism, where the term resonance is used in the following sense. As we saw in figure 13(*a*), when H_u and H_d have different values, the instability mode is similar to a single-interface mode. It consists of a strong region of perturbation vorticity centred at one interface, with a second, weaker and opposite rotation at the other interface. Since single-interface modes are generated at both of the interfaces, as the values of H_u and H_d approach each other, the strong perturbation vorticity of each single-interface mode might be amplified by the weaker, opposite sign vorticity of the single-interface mode from the opposite interface. Figure 13(*b*) shows the perturbation streamlines for such a configuration. We note that in this symmetrical case both interfaces are unstable and that the two perturbed vortices have equal strength. Hence, the two single-interface modes effectively amplify each other, thereby strengthening the symmetrical 'bamboo' mode.

The second island of instability, denoted by 'E' in figure 12, signifies an 'elliptical' instability in the sense discussed earlier. Indeed, this region is located precisely where Kliakhandler & Sivashinsky (1995) predicted it to be (see their figure 2*a*). The streamfunction eigenmode shows a phase shift between the perturbations of the two interfaces; see figure 13(*c*). There is only one circulation flow present, centred within the less viscous fluid. A change in the thickness of one of the interfaces does not have a strong effect on the growth rate, as can be seen in figure 14.

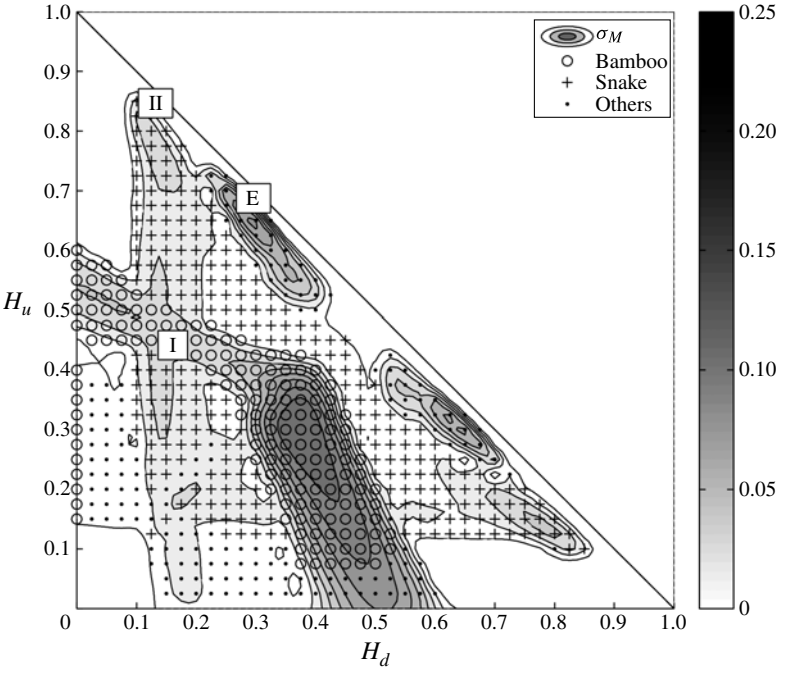

FIGURE 14. Growth rate of the most unstable mode as a function of the upper and lower fluid layer heights. The parameters are $R = 2.5$, $Re = 0$, $Pe = 2{,}000$, $\delta_u = 0.04$ and $\delta_d = 0.01$.

The last island of instability, marked 'II' in the figure, is more difficult to characterize. The streamfunction eigenmode in figure 13(*d*) seems to suggest that this mode is an interfacial instability. Surprisingly, however, a decrease of the interface thickness does not have a strong effect on the growth rate. By increasing the Péclet number, on the other hand, we can show that this mode is similar to the I_2-mode described in the previous section.

We now consider the stability diagram for the opposite case, i.e. when the more viscous fluid is located in the channel centre: see figure 15. Again, different instability modes can be identified. By inspecting the streamfunction eigenmode (figure 16) and changing one interface thickness (figure 17), one finds that I and II represent diffusive interfacial instabilities. I is a one-interface I_1-mode (two convections rolls), for which the other interface (close to the wall) has very little influence. Mode II is similar in nature to the I_2-mode, even though streamlines cross both interfaces. We note that, in contrast to the previous case, no resonance effects occur for the symmetric configuration. This is because the second interface does not have a vortex. While mode B is also a one-interface mode, it corresponds to the B_2-mode, as can be seen in figure 16. The last mode, denoted by E in the diagram, is more complex to characterize. The location in the diagram and the small influence of diffusion are similar to the E regime in the $R = 2.5$ case, when the less viscous fluid is in the centre. It is worth mentioning that if we increase the Péclet number, all modes except E vanish. Recall that the long-wave analysis of Kliakhandler & Sivashinsky (1995) does not predict any instabilities for $R < 0$. However, the streamfunction eigenmode in figure 16(*d*) shows that the wavelength is very small ($\alpha_M = 10.4$ in this case). It also displays a phase shift between the two interfaces, and a closed streamline region

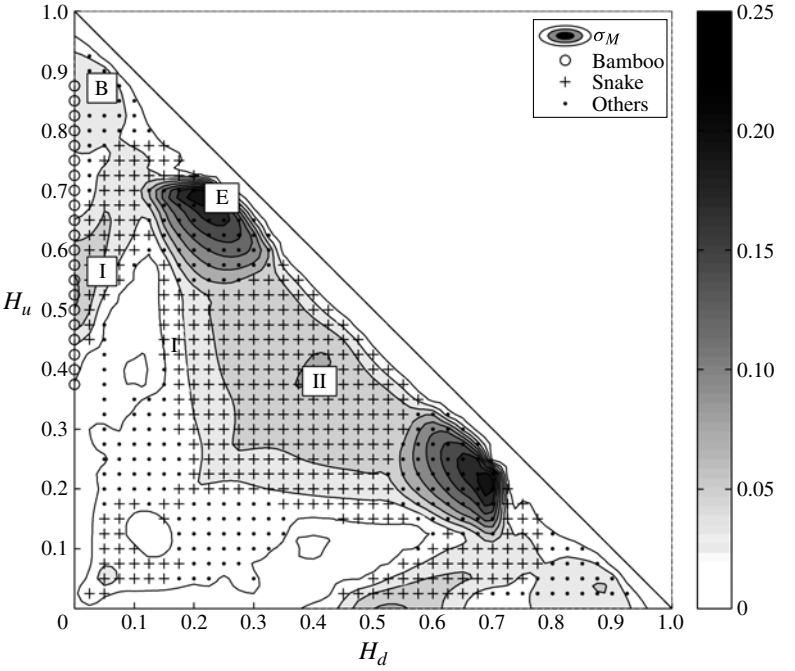

FIGURE 15. Growth rate of the most unstable mode as a function of the upper and lower fluid layer thicknesses. The parameters are $R = -2.5$, $Re = 0$, $Pe = 2{,}000$ and $\delta_u = \delta_d = 0.01$.

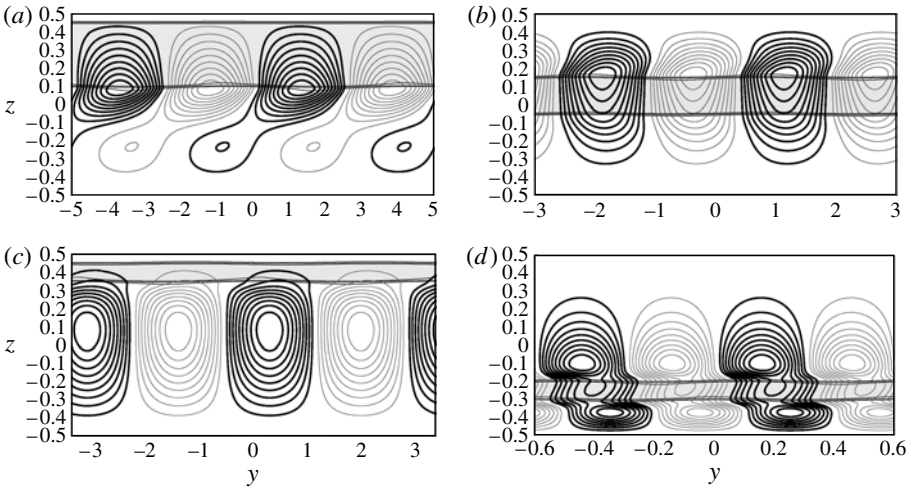

FIGURE 16. Streamfunction eigenmodes. The parameters are $Re = 0$, $R = -2.5$, $Pe = 2{,}000$, $\delta_u = \delta_d = 0.01$. (*a*) I-mode, $(H_d; H_u) = (0.6; 0.05)$, $\alpha_M = 1.2507$. (*b*) II-mode, $(H_d; H_u) = (0.45; 0.35)$, $\alpha_M = 2.0926$. (*c*) B-mode, $(H_d; H_u) = (0.85; 0.05)$, $\alpha_M = 1.8545$. (*d*) E-mode, $(H_d; H_u) = (0.2; 0.7)$, $\alpha_M = 10.4$.

centred between the two interfaces. In contrast to the previous E-mode, the instability involves three regions of closed streamlines.

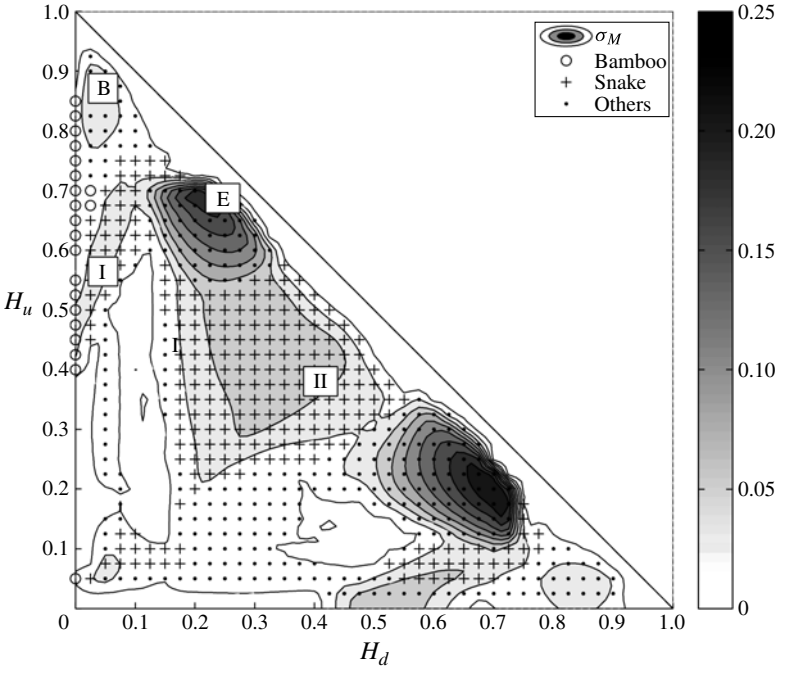

FIGURE 17. Growth rate of the most unstable mode as a function of the width of the upper and lower layer. The parameters are $R = -2.5$, $Pe = 2{,}000$, $\delta_u = 0.04$ and $\delta_d = 0.01$.

5. Conclusion

The results obtained in the present investigation demonstrate that diffusion in viscosity-layered Poiseuille flow can have a destabilizing effect very similar to that of inertia. We specifically focus on the Stokes flow limit in order to be able to address the influence of inertia and diffusion separately. The parametric study identifies four types of instability, each of which can dominate, depending on the interface locations. While the two dominant modes are interfacial in nature, the two bulk modes have much smaller growth rates. Our results show that the Péclet and Reynolds numbers affect the same unstable mode in a similar fashion. As suggested by Craik (1969), this may be related to the similar ways in which these two parameters appear in the perturbation equations. The convection–diffusion equation for the concentration perturbation also gives rise to a diffusive critical layer, where diffusion cannot be neglected. Regarding the physical mechanism responsible for the instability, this suggests that similar effects may be at work as for inertial instabilities. Govindarajan (2004) identifies an 'overlap' mode, which results in instability when the wave velocity is equal to the fluid velocity at the interface. For the present diffusive situation, a critical layer could in principle also exist. However, the above analysis shows the phase velocity of unstable perturbations to be quite different from the fluid velocity at the diffusive interface, so this critical layer mechanism does not seem to be relevant here. The 'bulk' modes identified above appear to be the diffusive analogues to the one observed by Wall & Wilson (1996). Using similar arguments to those of Hinch (1984), we propose a mechanism for the destabilization of miscible Stokes flows. As for immiscible flows, we find that the perturbation vorticity and the associated velocity generated at the interface have a phase shift with regard to the interface perturbation.

This vorticity thus destabilizes the interface by amplifying the crests and valleys of the interface. The mechanism that produces the phase shift must be different from the one described by Hinch (1984) for immiscible flows, since there is no inertia in the momentum equations. Here the shift is produced by the convection and diffusion of the perturbed concentration, and thus viscosity.

Three-layered Stokes flows are also found to be unstable. For such flows, we observe modes that correspond to their two-layer counterparts, with some modification due to the presence of the second interface. In addition, we find that the two interface modes can be in resonance, thereby enhancing the growth rate. Interestingly, the symmetric Poiseuille flow case ($H_u = H_d$) gives rise only to instabilities of the diffusive 'I'-mode for $R = \pm 2.5$. This suggests that a corresponding axisymmetric mode may be responsible for the observation by Selvam *et al.* (2007) of a pipe flow instability in the vanishing *Re* regime.

For three-layer Poiseuille flow, we also observe additional instability modes that are not due to diffusion. Some of these modes are consistent with predictions from long-wavelength stability analyses of two non-diffusive sharp interfaces by Li (1969), Kliakhandler & Sivashinsky (1995) and Shariati *et al.* (2004). However, while those long-wavelength analyses predict instabilities only for $R > 0$, the present analysis, which covers all wavenumbers, demonstrates that unstable modes also exist for $R < 0$, albeit at much smaller wavelengths. It is interesting to note that these instability modes require the presence of at least two interfaces, due to the reversibility of the Stokes equation. This is consistent with the fact that we observe only diffusive modes for two-layered systems.

It will be interesting to extend the present investigation to diffusive instabilities in related geometries such as Couette or mixed Poiseuille/Couette flows. In fact, the striking similarities between the present findings and those of Ern *et al.* (2003) suggest that the mechanisms described here could be responsible for some of their observations, in particular for the non-monotonic behaviour of the growth rate as a function of the Péclet number. Finally, we need to keep in mind that the present stability analysis is based on the assumption of a uniform and stationary base state. This represents an approximation, as in a real flow the base state evolves in space and time due to diffusion. Hence, future work should address the spatial stability analysis along the lines explored by d'Olce *et al.* (2009), Sahu *et al.* (2009) and Selvam *et al.* (2009), in order to understand the contribution of the diffusive mode on the transition from convective to absolute instability. Finally, it will be of interest to explore the nonlinear behaviour (see Charru & Fabre 1994) to derive the contribution of miscibility on the equation of motion of the pseudo-interface. Fully nonlinear Stokes simulations will be useful in this context.

E.M. gratefully acknowledges support through NSF grant CTS-0456722. L.T. was partially funded by the French Ministry of Foreign Affairs through the Lavoisier fellowship program.

REFERENCES

CHARRU, F. & FABRE, J. 1994 Long waves at the interface between two viscous fluids. *Phys. Fluids* **6**, 1223–1235.

CHARRU, F. & HINCH, E. J. 2000 'Phase diagram' of interfacial instabilities in a two-layer Couette flow and mechanism of the long-wave instability. *J. Fluid Mech.* **414**, 195–223.

CRAIK, A. D. D. 1969 The stability of plane Couette flow with viscosity stratification. *J. Fluid Mech.* **36**, 685–693.

DRAZIN, P. G. & REID, W. H. 1981 *Hydrodynamic Stability*. Cambridge University Press.

ERN, P., CHARRU, F. & LUCHINI, P. 2003 Stability analysis of a shear flow with strongly stratified viscosity. *J. Fluid Mech.* 295–312.

GOVINDARAJAN, R. 2004 Effect of miscibility on the linear instability of two-fluid channel flow. *Intl J. Multiphase Flow* **30**, 1177–1192.

HICKOX, C. E. 1971 Instability due to viscosity and density stratification in axisymmetric pipe flow. *Phys. Fluids* **14**, 251.

HINCH, E. J. 1984 A note on the mechanism of the instability at the interface between two shearing fluids. *J. Fluid Mech.* **144**, 463–465.

HOOPER, A. P. & BOYD, W. G. C. 1983 Shear-flow instability at the interface between two fluids. *J. Fluid Mech.* **128**, 507–528.

JOSEPH, D. D. 1968 Eigenvalue bounds for the Orr–Sommerfeld equation. *J. Fluid Mech. Digital Archive* **33**, 617–621.

JOSEPH, D. D. & RENARDY, Y. Y. 1992*a* *Fundamentals of Two-Fluid Dynamics. Part I. Mathematical Theory and Applications*. Springer.

JOSEPH, D. D. & RENARDY, Y. Y. 1992*b* *Fundamentals of Two-Fluid Dynamics. Part II. Lubricated Transport, Drops and Miscible Liquids*. Springer.

KLIAKHANDLER, I. & SIVASHINSKY, G. 1995 Kinetic alpha effect in viscosity stratified creeping flow. *Phys. Fluids* **7**, 1866–1871.

LELE, S. K. 1992 Compact finite difference schemes with spectral-like resolution. *J. Comput. Phys.* **103**, 16–42.

LI, C.-H. 1969 Instability of three-layer viscous stratified flow. *Phys. Fluids* **12**, 2473–2481.

LIN, C. C. 1955 *The Theory of Hydrodynamic Stability*. Cambridge University Press.

MACK, I. M. 1976 A numerical study of the temporal eigenvalue spectrum of Blasius boundary layer flow. *J. Fluid Mech.* **73**, 497–520.

MALIK, S. V. & HOOPER, A. P. 2005 Linear stability and energy growth of viscosity stratified flows. *Phys. Fluids* **17**, 024101.

NOUAR, C. & FRIGAARD, I. 2009 Stability of plane Couette–Poiseuille flow of shear-thinning fluid. *Phys. Fluids* **21**, 064104.

D'OLCE, M., MARTIN, J., RAKOTOMALALA, N., SALIN, D. & TALON, L. 2008 Pearl and mushroom instability patterns in two miscible fluids core annular flow. *Phys. Fluids* **20**, 24104.

D'OLCE, M., MARTIN, J., RAKOTOMALALA, N., SALIN, D. & TALON, L. 2009 Convective/absolute instability in miscible core–annular flow. Part 1. Experiments. *J. Fluid Mech.* **618**, 305–311.

RANGANATHAN, B. T. & GOVINDARAJAN, R. 2001 Stabilization and destabilization of channel flow by the location of viscosity-stratified fluid layer. *Phys. Fluids* **13** (1), 1–3.

RENARDY, Y. 1987 Viscosity and density stratification in vertical Poiseuille flow. *Phys. Fluids* **30**, 1638.

SAHU, K. C., DING, H., VALLURI, P. & MATAR, O. K. 2009 Linear stability analysis and numerical simulation of miscible two-layer channel flow. *Phys. Fluids* **21**, 042104.

SCHMID, P. J. & HENNINGSON, D. S. 2001 *Stability and Transition in Shear Flows*. Springer.

SCOFFONI, J., LAJEUNESSE, E. & HOMSY, G. M. 2001 Interface instabilities during displacement of two miscible fluids in a vertical pipe. *Phys. Fluids* **13**, 553–556.

SELVAM, B., MERK, S., GOVINDARAJAN, R. & MEIBURG, E. 2007 Stability of miscible core–annular flow with viscosity stratification. *J. Fluid Mech.* **592**, 23–49.

SELVAM, B., TALON, L., LESSHAFT, L. & MEIBURG, E. 2009 Convective/absolute instability in miscible core–annular flow. Part 2. Numerical simulation and nonlinear global modes. *J. Fluid Mech.* **618**, 323–348.

SHARIATI, M., TALON, L., MARTIN, J., RAKOTOMALALA, N., SALIN, D. & YORTSOS, Y. C. 2004 Fluid displacement between two parallel plates: a non-empirical model displaying change of type from hyperbolic to elliptic equations. *J. Fluid Mech.* **519**, 105–132.

SOUTH, M. J. & HOOPER, A. P. 1999 Linear growth in two-fluid plane Poiseuille flow. *J. Fluid Mech.* **381**, 121–139.

TALON, L., MARTIN, J., RAKOTOMALALA, N., SALIN, D. & YORTSOS, Y. C. 2004 Crossing the elliptic region in a hyperbolic system with change-of-type behaviour, arising in flow between two parallel plates. *Phys. Rev.* E **69**, 066318.

WALL, D. P. & WILSON, S. K. 1996 The linear stability of channel flow of fluid with temperature-dependent viscosity. *J. Fluid Mech.* **323**, 107–132.

YANG, Z. & YORTSOS, Y. C. 1997 Asymptotic solutions of miscible displacements in geometries of large aspect ratio. *Phys. Fluids* **9**, 286–298.

YIANTSIOS, S. G. & HIGGINS, B. G. 1988 Linear stability of plane Poiseuille flow of two superposed fluids. *Phys. Fluids* **31**, 3225–3238.

YIH, C. S. 1967 Instability due to viscosity stratification. *J. Fluid Mech.* **27**, 337–352.